

OmniCount: Multi-label Object Counting with Semantic-Geometric Priors

Anindya Mondal^{123*}, Sauradip Nag^{125*}, Xiatian Zhu¹²³, Anjan Dutta¹²³⁴

¹University of Surrey, ²CVSSP, ³Surrey Institute for People-Centred AI,

⁴School of Veterinary Medicine, ⁵iFlyTek-Surrey Joint Research Center on AI

{a.mondal, s.nag, xiatian.zhu, anjan.dutta}@surrey.ac.uk,

*Equal Contribution

Abstract. Object counting is pivotal for understanding the composition of scenes. Previously, this task was dominated by class-specific methods, which have gradually evolved into more adaptable class-agnostic strategies. However, these strategies come with their own set of limitations, such as the need for manual exemplar input and multiple passes for multiple categories, resulting in significant inefficiencies. This paper introduces a new, more practical approach enabling simultaneous counting of multiple object categories using an open vocabulary framework. Our solution, OmniCount, stands out by using semantic and geometric insights from pre-trained models to count multiple categories of objects as specified by users, all without additional training. OmniCount distinguishes itself by generating precise object masks and leveraging point prompts via the Segment Anything Model for efficient counting. To evaluate OmniCount, we created the OmniCount-191 benchmark, a first-of-its-kind dataset with multi-label object counts, including points, bounding boxes, and VQA annotations. Our comprehensive evaluation in OmniCount-191, alongside other leading benchmarks, demonstrates OmniCount’s exceptional performance, significantly outpacing existing solutions and heralding a new era in object counting technology.

1 Introduction

Understanding the distribution of objects in a scene through counting across multiple categories is essential for comprehensive scene analysis. Traditionally, object counting has been constrained to class-specific methodologies, each tailored to distinct categories such as crowds [11, 13, 20, 21, 24, 27, 44], cells [17], fruits [34], and vehicles [2]. However, the quest for greater versatility has led to the advent of class-agnostic models, capable of adapting to count objects across varied scenes – from biological slides to celestial bodies [3, 15, 35, 37, 52]. Despite their innovative approach, these models are constrained by their reliance on manual inputs of exemplars and the necessity for separate processing for each object category, leading to increased computational demands and reduced practicality. Whilst this limitation could be mitigated by counting multiple categories via detection and/or instance segmentation [3, 7, 8], dealing with small-sized or

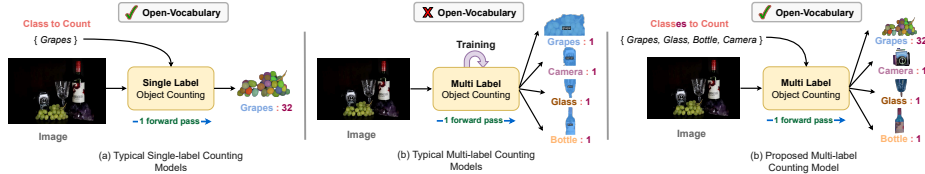


Fig. 1: Object counting paradigms: (a) Typical single-label object counting models supports open-vocabulary counting but processes only *a single category* one time. (b) Existing multi-label object counting models are training based (i.e., not open-vocabulary) approaches and also fail to count *non-atomic objects* (e.g., grapes). (c) We advocate more efficient and convenient *multi-label counting* that is training-free, open-vocabulary and supports counting all the target categories in a single pass.

non-atomic objects—those typically referred to collectively, such as grapes or bananas (more discussions on the supplementary material)—is still largely limited as these sorts of objects are often too hard to detect.

Inspired by the above observations and insights, we introduce **OmniCount**, a novel, training-free approach that leverages open vocabulary to enable efficient and simultaneous counting of multiple object categories. OmniCount distinguishes itself by utilizing semantic and geometric cues from pre-trained models to partition images into semantically coherent regions, employing depth cues to identify occluded objects, and ensuring precise object delineation. A key feature of OmniCount is its application of k -nearest neighbors-based geometric corrections along the edges of semantic masks, which promotes category exclusivity and depth consistency. This strategy not only refines segmentation to prevent overlap but also enables the effective use of existing segmentation models, such as the Segment Anything Model (SAM) [18], to generate individual object masks for counting across the required categories. Given that SAM uniquely enables fine-grained and non-atomic object segmentation using points as segmentation prompts, it was selected as our preferred segmentation module for counting.

As an under-studied object counting problem, there is no ready-to-use dataset featuring annotations for multiple generic categories per image. Besides, sparsely populated object detection datasets like PASCAL VOC [9] and MS COCO [26] cannot adequately represent real-world counting challenges. The absence of a suitable dataset for this underexplored domain prompted the creation of the **OmniCount-191** benchmark. This comprehensive dataset includes 3,02,300 object instances across 191 categories in 30,230 images, featuring a rich array of annotations, including counts, points, bounding boxes, and segmentation masks, thus establishing a new benchmark for object counting challenges. This dataset features not only multiple categories per image but also a variety of detailed annotations such as counts, points, bounding boxes, and segmentation masks for each object (Fig. 5).

In summary, we make the following contributions: (1) We re-promote multi-label object counting that bypasses the conventional reliance on object detection and semantic segmentation models, addressing common accuracy issues such as over and undercounting; (2) We introduce a novel, efficient, and user-friendly

framework **OmniCount** for multi-label object counting that utilizes semantic and geometric cues without necessitating additional training; (3) We create a new multi-label object counting dataset, **OmniCount-191**, with rich annotations for fostering the development of this newly introduced setting; (4) We conduct extensive experiments to demonstrate OmniCount’s superior performance over existing methodologies on our dataset and other established benchmarks.

2 Related Work

Learning-based object counting: Traditional counting methods have focused on specific categories like crowds [11, 13, 20, 21, 24, 27, 44], cells [17], fruits [34], and vehicles [2], primarily through regression-based techniques to create density maps from point annotations [4–6, 19, 22, 23, 40, 43, 49, 50, 58]. Density-based counting requires point annotations for each countable object in training images, which are then used to generate density maps via Gaussian convolution. A model is then trained to predict a density map for each input image, and the object count is obtained by summing the pixel values in the predicted density map. This class-specific approach is effective for its trained categories but lacks the flexibility for broader applications. In contrast, class-agnostic counting aims for versatility, using exemplars to count objects of any category [10, 30, 36, 38, 39, 41, 45, 51, 53, 55–57]. These methods adapt by learning from similarity maps, offering a dynamic solution for counting across arbitrary classes.

Given the intensive requirement for annotated training data in density-based counting, which is both time-consuming and challenging to scale, we propose a novel approach – a training-free object counter. It allows object counting using prompts like points, boxes, or text, eliminating the need for training. This approach broadens the possibilities for counting objects in diverse scenarios without the data collection and counting-specific training burden.

Multi-label object counting: Despite the advancements in single-label counting, real-world scenarios often involve scenes with multiple object classes coexisting [52, 53]. Prior work by Cholakal *et al.* [7, 8] and Chattopadhyay *et al.* [3] has explored multi-label counting in sparse settings, focusing on global counts and labels within human discernible ranges. However, these methods struggle to identify non-atomic or densely clustered objects, such as grapes. Few-shot counting [37] attempts to address denser scenarios but typically restricts to one category per image. Our work underscores the necessity for datasets that accurately reflect the complexity of real-world scenes, supporting dense multi-class object interactions.

Prompt-based foundation model: The introduction of large language models, notably GPT [1], has ushered in a new era in natural language processing and computer vision, showcasing extraordinary generalization capabilities in zero-shot and few-shot scenarios. Foundation models, such as CLIP [33], utilize contrastive learning to synchronize text and image encoders, adeptly handling new visual concepts via textual prompts and demonstrating unparalleled zero-shot transfer capabilities across various visual domains.

In the realm of image segmentation, the Segment Anything Model (SAM) [18] represents a significant advancement, catering to a wide range of prompts like

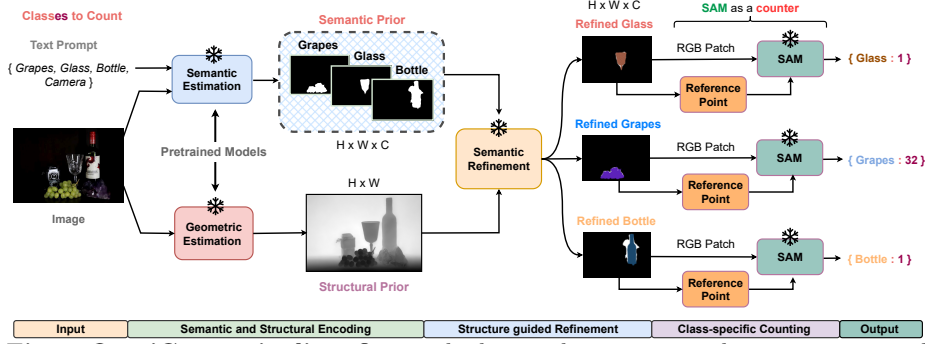


Fig. 2: OmniCount pipeline: Our method starts by processing the input image and their target object classes, using Semantic Estimation (SAN [47]) and Geometric Estimation (Marigold [16]) modules to generate class-specific masks and depth maps. These initial priors are refined with a Semantic Refinement module for accuracy, creating precise binary masks of target objects. The refined masks help in obtaining RGB patches for each class and also extracting reference points to reduce overcounting. SAM uses these RGB patches and reference points to create instance-level masks, yielding precise object counts. * represents frozen pre-trained models.

points, boxes, and text to generate precise object masks. This model excels in various segmentation benchmarks, illustrating robust zero-shot transfer abilities across diverse datasets. The notion of an ideal object counter encompasses attributes like *visual promptability*, enabling the model to respond to visual cues interactively; *interactiveness*, allowing users to guide the counting process; and *open-set* counting capabilities, ensuring the model can count objects of any category. While SAM embodies these characteristics, making it a potent tool for interactive segmentation, its application in object counting faces challenges with occluded scenes [14] and multi-class object counting [42] due to its class-agnostic approach. We tackle these limitations by integrating depth and semantic priors into SAM’s framework, thus enhancing its functionality for complex counting tasks in scenarios with occlusions and multiple object classes and fully realizing the concept of an ideal counting model.

3 OmniCount

In this work, we aim to achieve open-vocabulary, multi-label training-free object counting within a given image and with a set of labels to be counted in that image. An illustration of our proposed model is provided in Fig. 2. We begin our discussion by defining the multi-label counting problem in Sec. 3.1. Our proposed approach leverages semantic and geometric priors, which are respectively derived via Semantic and Geometric Estimation modules, as elaborated in Sec. 3.2. A Semantic Refinement module that enhances the initial semantic mask with geometric information is detailed in Sec. 3.3. Finally, we consider the feature representation from semantic priors to select fine-grained reference points for the objects and then employ SAM [18] for obtaining fine-grained masks for counting objects for each category, which is described in Sec. 3.4.

3.1 Problem formulation

The problem of multi-label object counting can be defined as obtaining an object counter $\mathcal{F}_{\text{count}}$ using a training set $\mathcal{D}_{\text{train}} = \{(I_1, \mathcal{P}_1, \mathcal{C}_1), \dots, (I_N, \mathcal{P}_N, \mathcal{C}_N)\}$, where each $I_i \in \mathbb{R}^{H \times W \times 3}$ represents an RGB image, $\mathcal{P}_i = \{p_1, \dots, p_{m_i}\}$ is a set of class labels and $\mathcal{C}_i = \{c_1, \dots, c_{m_i}\}$ are the corresponding object counts (*i.e.* object with label p_k occurs c_k times in I_i), with m_i being the number of unique objects in the i -th image and N the total number of training data points in $\mathcal{D}_{\text{train}}$. For a given image I_k and a subset of class labels $\{p_1, \dots, p_{k_l}\} \subseteq \mathcal{P}_k$, the function $\mathcal{F}_{\text{count}}$ should result in the following:

$$\{c_1, \dots, c_{k_l}\} = \mathcal{F}_{\text{count}}(I_k, \{p_1, \dots, p_{k_l}\}) \quad (1)$$

where c_{k_l} is the number of occurrences of the object with label p_{k_l} in the image I_k . Our goal is to develop an open-vocabulary multi-label object counting model $\mathcal{F}_{\text{count}}$, such that it generalizes well to $\mathcal{D}_{\text{test}}$, a held-out test set of data points with classes not in $\mathcal{D}_{\text{train}}$, *i.e.* $\mathcal{D}_{\text{train}} \cap \mathcal{D}_{\text{test}} = \emptyset$. To achieve this, we introduce OmniCount, a multi-label object counting model that utilizes semantic and geometric priors to avoid training that usually requires large datasets and expensive computational resources. Since our model is training-free, we do not use $\mathcal{D}_{\text{train}}$ and only evaluate our model on $\mathcal{D}_{\text{test}}$.

3.2 Semantic and Structural Encoding

Semantic Estimation Module: Prior research in object counting [36, 42, 45, 46] has predominantly focused on single-class scenarios. Yet, real-world scenes often comprise multiple object categories, necessitating semantic understanding for accurate counting. This semantic information can be obtained using any standard open-vocabulary segmentation model [25, 32, 47, 48]. In this paper, we utilize the Side Adapter Network (SAN) [47] as a semantic segmentation model \mathcal{E}_{sem} that takes an image I and a set of class labels $\mathcal{P} = \{p_1, \dots, p_m\}$ as input and results in $\mathbf{S}_{\mathcal{P}} = \{S_1, \dots, S_m\}$, a set of binary semantic masks corresponding to the classes in \mathcal{P} as follows:

$$\mathbf{S}_{\mathcal{P}}, F_{\mathcal{P}} = \mathcal{E}_{\text{sem}}(I, \mathcal{P}) \quad (2)$$

where $F_{\mathcal{P}} \in \mathbb{R}^{\frac{H}{K} \times \frac{W}{K} \times C}$ is an intermediate low-resolution feature activations, with K and C being integers depending on the design of \mathcal{E}_{sem} . We use $\mathbf{S}_{\mathcal{P}}$ as a semantic prior, essentially bridging the gap between multi-label counting and semantic awareness. However, while segmenting 2D RGB images, SAM [18] primarily relies on texture information, such as color, which, when coupled with occlusion, leads to over-segmenting masks (see Fig. 2 for “bottle” class) and consequently, over-counting. Thus, the challenge is to obtain fine-grained segmentation results by integrating more geometric information to mitigate the over-segmentation and over-counting issue. We reduce the over-segmentation issue by using a refinement of the segmentation mask based on geometric priors (discussed in the

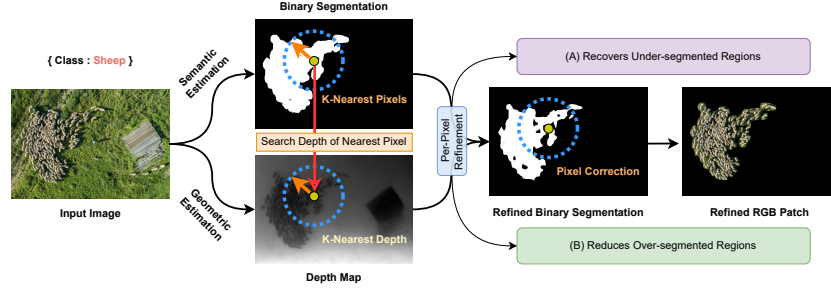


Fig. 3: Geometry aware Object Semantics Refinement: We refine semantic masks with geometric priors, using k-nearest neighbor searches to filter edge pixels by category uniqueness and depth alignment, enhancing mask precision through depth-integrated segmentation.

next paragraph). To further reduce the over-counting issue, we use the intermediate low-resolution feature activations $F_{\mathcal{P}}$ to select the most probable reference points (discussed in Sec. 3.4) belonging to the object. Thereafter, SAM uses refined segmentation masks and reference points to segment accurate object masks.

Geometric Estimation Module: Classical segmentation models [18, 29] mostly leverage texture information for object delineation, but this approach falls short in accurately localizing objects under significant occlusion. Counting dense interacting or overlapping objects requires information beyond RGB. We draw inspiration from the remarkable ability of humans to identify objects by visualizing depth maps. Compared to RGB images, the rendered depth image ignores the texture information and utilizes structural information in segmenting objects near or far away from the camera without class information, as shown in Fig. 2. Thus, it serves as a structural/geometric prior for the coarse segmentation masks that help recover undiscovered objects or refine object semantics. Using an off-the-shelf depth map rendering model Marigold [16] denoted by $\mathcal{E}_{\text{depth}}$, we generate depth map D for the image I as $D = \mathcal{E}_{\text{depth}}(I)$, which serve as geometric prior for our model. Notably, D is a matrix of the same spatial dimension as the image I , with pixels having normalized depth values in $[0, 1]$. This implies that for a pixel $x \in I$, $D(x) \in [0, 1]$ indicates the normalized depth value of x . We utilize this pixel-wise depth information to refine the coarse segmentation mask $\mathbf{S}_{\mathcal{P}}$, which is discussed in the following subsection.

3.3 Geometry aware Object Semantics Refinement

To minimize overcounting using SAM as a counter, we obtain fine-grained semantic masks by injecting geometric priors before passing them into SAM. To refine the semantic prior $\mathbf{S}_{\mathcal{P}}$ with geometric insights from the depth prior D , we conduct a k-nearest neighbor (kNN) (refer to Fig. 3) search centering around each of the pixels of the individual semantic mask to ensure two conditions are met:

- (1) A pixel must exclusively belong to its designated object category, preventing

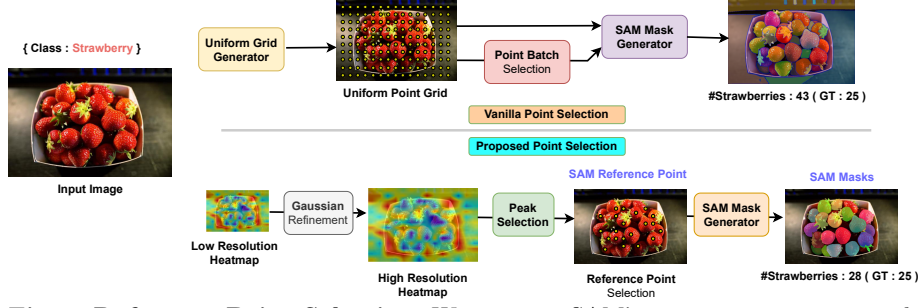


Fig. 4: Reference Point Selection: We improve SAM’s segmentation accuracy by refining reference points with semantic priors, identifying local maxima, and applying Gaussian refinement to address misalignment and quantization errors. The refined points merged with a semantic mask through the Hadamard product, concentrating segmentation on foreground objects, enhancing mask precision and object counting accuracy while addressing the limitations of SAM’s default “everything mode” mode.

any overlapping with masks of other categories. For a pixel x in mask S_j :

$$C_1(x) : x \notin S_k, \forall k \neq j$$

(2) The absolute difference between a pixel’s depth and the mean depth of its object category must fall below a specified tolerance τ , ensuring depth consistency (for objects with curved edges). For a pixel x in S_n with mean depth $D_\mu(S_n)$:

$$C_2(x) : |D(x) - D_\mu(S_n)| < \tau$$

where $D(x)$ denotes the depth of pixel x and $D_\mu(S_n) = \frac{1}{s} \sum_y D(y), \forall y \in S_n$ with s as the total number of pixels in S_n . Pixels that fulfill both conditions $C_1(x)$ and $C_2(x)$ are integrated into their appropriate object class, leading to a refined semantic prior $\mathbf{S}'_{\mathcal{P}}$, computed as $\mathbf{S}'_{\mathcal{P}} = \mathcal{R}_{\text{geom}}(\mathbf{S}_{\mathcal{P}}, D)$, where $\mathcal{R}_{\text{geom}}$ is the geometry-aware semantic refinement function, enhancing the precision of the semantic masks by considering depth information. This depth-aware refined mask (refer to Fig. 3) minimizes the risk of over-segmentation (see Tab. 4) or recovers undiscovered objects in occluded scenes.

3.4 SAM as a counter

SAM [18] integrates an image encoder for extracting features from images, a prompt encoder for interpreting textual, point, or box prompts, and a mask decoder that utilizes these encoded representations to generate segmentation masks. Vanilla SAM uses a point grid generator (in “everything mode”) to lay uniform points all over the image before generating masks for each of such points. This results in point placement in the foreground and background of the target object, leading to the generation of irrelevant background masks and overcounting.

Reference point selection: To mitigate the overcounting issue in SAM, we refine the process of selecting reference points (refer to Fig. 4) for the SAM decoder

using the feature activations $F_{\mathcal{P}}$ from semantic priors (see Eq. (2)). Specifically, we utilize $F_{\mathcal{P}}$ to enhance the accuracy of text-image similarity computations. A set of reference points $\mathbf{P} = \{\rho_1, \dots, \rho_s\}$ are then selected by identifying local maximas within $F_{\mathcal{P}}$. However, due to the low resolution of $F_{\mathcal{P}}$, direct upsampling to image resolution can lead to misalignment [54] due to quantization errors (refer to Tab. 4), making these points unsuitable for mask generation. To address this, we apply Gaussian refinement to the low-resolution reference points \mathbf{P} , inspired by [54], minimizing quantization errors during upsampling. The corrected reference points are denoted as $\mathbf{P}' = \{\rho'_1, \dots, \rho'_s\}$. To specifically target foreground objects and avoid background segmentation, we compute the Hadamard product between the refined semantic mask S'_m for class p_m and the corrected reference points \mathbf{P}' as $\mathbf{Q}_m = S'_m \circ \mathbf{P}'$, where \circ represents the Hadamard product, and $\mathbf{Q}_m \subseteq \mathbf{P}'$ denotes the set of resulting reference points for objects belonging to the label p_m , serving as a guide for identifying regions likely to contain the target objects, as illustrated in Fig. 4. Notably, this automated selection of reference points can be replaced by point or box annotations provided as input to the SAM decoder, thus making our model interactive to multiple user inputs.

SAM Mask Generator: By incorporating the reference object activation $F_{\mathcal{P}}$ and modifying the mask generation process as mentioned, the mask decoder of SAM can now focus more attentively on the reference object feature. This inclusion of additional contextual information through $F_{\mathcal{P}}$ greatly assists the mask generator in accurately distinguishing and segmenting the target objects within the image. Since SAM’s encoder expects an RGB image as input, we obtain an RGB patch I_m of the target object by multiplying the input image I and refined semantic mask S'_m (see Fig. 3). We then obtain the resultant mask \mathbf{M}_m from SAM as $\mathbf{M}_m = \text{SAM}(I_m, \mathbf{Q}_m)$, where $\mathbf{M}_m = \{M_{m_1}, \dots, M_{m_n}\}$ is the set of individual object masks segmented by SAM; we count these masks to find the total number of objects belonging to the class label p_m . Leveraging these priors enables focusing on the targeted objects without segmenting unrelated entities. This targeted approach enhances efficiency and accuracy beyond the standard “segment everything” strategy, which involves applying uniform grids over the image. Finally, the masks that are empty or cover an insignificantly small area are discarded, creating a refined subset $\mathbf{N}_m \subseteq \mathbf{M}_m$, which contains only the significant masks for the final tally of objects. The cardinality of \mathbf{N}_m , $\text{card}(\mathbf{N}_m)$, denotes the final count of objects of class-label m in image I .

4 OmniCount-191 dataset

To effectively evaluate OmniCount across open-vocabulary, supervised, and few-shot counting tasks, a dataset catering to a broad spectrum of visual categories and instances featuring various visual categories with multiple instances and classes per image is essential. The current datasets, primarily designed for object counting [37] focusing on singular object categories like humans and vehicles, fall short for multi-label object counting tasks. Despite the presence of multi-class datasets like MS COCO [26], their utility is limited for counting due to the sparse

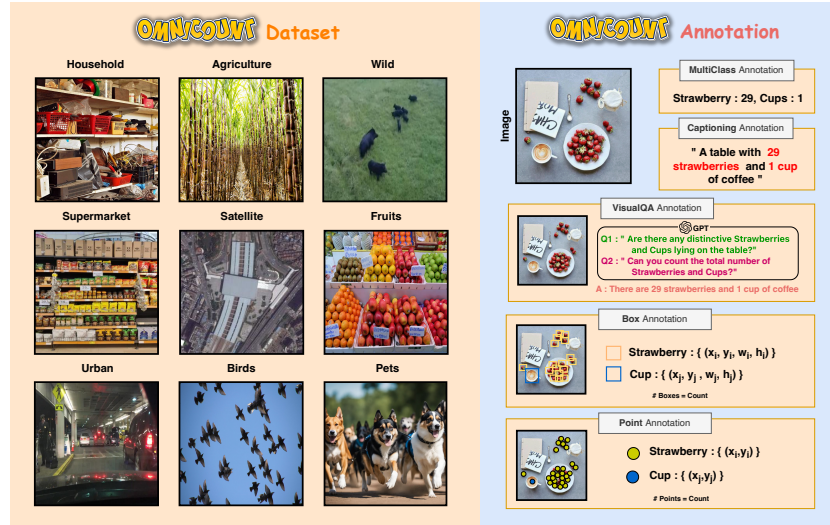


Fig. 5: OmniCount-191 Dataset: A collection of images having 191 classes across nine domains, with each image annotated with captions, VQA, boxes, and points.

nature of object appearance. Addressing this gap, we created a new dataset with 30,230 images spanning 191 diverse categories, including kitchen utensils, office supplies, vehicles, and animals. This dataset, as shown in Fig. 6, featuring a wide range of object instance counts per image ranging from 1 to 160 and an average count of 10, bridges the existing void and establishes a benchmark for assessing counting models in varied scenarios.

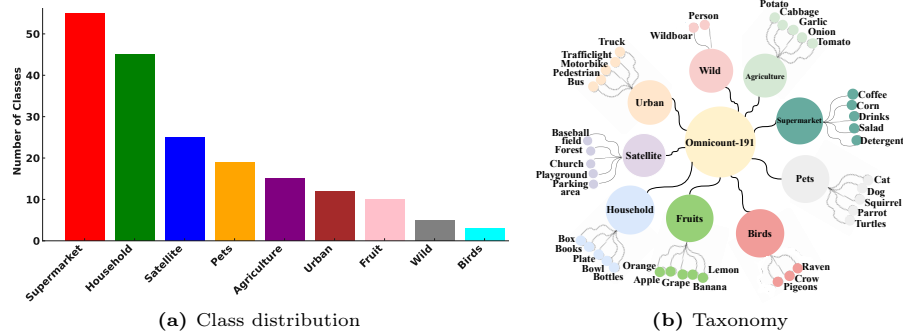


Fig. 6: A concise overview of the OmniCount-191 dataset: This dataset features images across nine diverse domains, encompassing a wide range of object densities, shapes, and sizes, making it perfectly suited for object counting tasks. The left figure shows the number of categories per domain, and the right one shows the most frequent object categories present per domain.

Image Collection: Our dataset, consisting of 30,230 images, was carefully collected to ensure utility and quality. It was curated from a broad collection of candidate images identified through keyword searches across 191 real-world ob-

ject categories. The selection was refined through a detailed manual review, adhering to stringent criteria: (1) **Object instances:** Each image must contain at least *five* object instances, aiming to challenge object enumeration in complex scenarios; (2) **Image quality:** High-resolution images were selected to ensure clear object identification and counting; (3) **Severe occlusion:** We excluded images with significant occlusion to maintain accuracy in object counting; (4) **Object dimensions:** Images with objects too small or too distant for accurate counting or annotation were removed, ensuring all objects are adequately sized for analysis. This selection process crafted a dataset poised to advance object counting algorithm development and testing, tailored for real-world applicability. **Dataset Statistics:** The OmniCount-191 benchmark, depicted in Figs. 5 and 6, presents images with small, densely packed objects from multiple classes, reflecting real-world object counting scenarios. This dataset encompasses 30,230 images, with dimensions averaging 700×580 pixels. Each image contains an average of 10 objects, totaling 302,300 objects, with individual images ranging from 1 to 160 objects. To ensure diversity, the dataset is split into training and testing sets, with no overlap in object categories – 118 categories for training and 73 for testing, corresponding to a 60%-40% split. This results in 26,978 images for training and 3,252 for testing. For specific applications, class splits are available for few-shot and zero-shot settings, detailed in the supplementary.

5 Experiments

Datasets: Given the limitations of existing datasets for precise multi-label object counting, we evaluate our model using the new OmniCount-191 benchmark, designed for multi-class counting. For a thorough and fair comparison, we also compare our OmniCount against previous works [3, 7] on the commonly used PASCAL VOC dataset. For single-class counting evaluation, we used the test set of FSC-147 [37] and CARPK [12] datasets. The FSC-147 test set comprises 1190 images across 29 categories. In contrast, PASCAL VOC offers 9963 images spanning 20 real-world classes, with 4952 designated for testing. CARPK, focusing on aerial car counting, includes 1014 test images. Both FSC-147 and CARPK provide point and box annotations compatible with our model, whereas PASCAL VOC only provides box annotations. For a fair comparison, we use the test splits of these datasets, similar to TFOC [42], ILC [7], and CEOS [3].

Evaluation metrics: For evaluating our model’s performance in single-class object counting, we employ four key metrics in line with leading benchmarks [36, 37, 42]: Mean Average Error (MAE) for standard accuracy assessment, Normalized Mean Average Error (NMAE) for a more intuitive understanding of errors, along with Normalized Relative Error (NAE) and Squared Relative Error (SRE) for comprehensive error analysis. In multi-label counting, we use mean-RMSE (mRMSE) and nonzero-RMSE (mRMSE-nz) to assess the model’s precision across various object categories, following the prior works [3, 7, 8].

Implementation details: In our experiments, we employ “ViT-Large” for SAN [47] and “ViT-Base” for SAM [18] models. For the k-nearest neighbor, we use a 10-

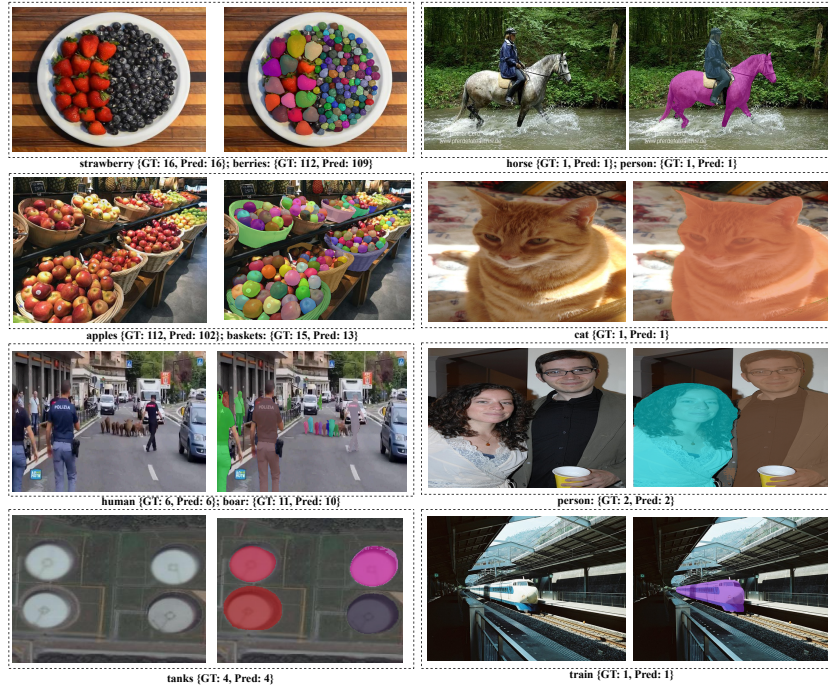


Fig. 7: Results using OmniCount: OmniCount-191 (left), PASCAL VOC (right).

pixel search window and set a depth threshold $\tau = 0.3$ to accommodate the depth variance of objects with curved edges. The values of K and C are respectively set as 16 and 256. For our prior-guided mask generation, we select the local maxima in SAN’s heatmap [47], then refine them using Gaussian refinement (see Sec. 3.3) with $\sigma = 0.4$ and $\omega = 4$. Finally, we input them as reference object points into SAM for mask generation and counting. Additionally, we compare box and point prompts with traditional counting methods [42]. For the former, bounding boxes from PASCAL VOC [9] and OmniCount-191 datasets serve as prompts for SAM. For datasets having no point annotation, we calculate the centroid of each bounding box and use its coordinates as prompts.

5.1 Multi-label counting

Competitors: For a fair comparison with state-of-the-art, we adapt the single-label object counting model TFOC [42] for multi-label counting by running it for each class in an image to obtain multi-label counts. We also replicate and evaluate the performance of ILC [8] for a direct comparison, while attempts to replicate CEOES [3] were limited by its Lua implementation. We additionally employ open-vocabulary object detection (Grounding-DINO [28]) and semantic segmentation (CLIPSeg [31]) baselines for multi-label object counting. The Grounding-DINO-based baseline counts objects by enumerating detected bounding boxes per category, whereas the CLIPSeg-based baseline uses a ViT encoder and spectral clustering to estimate category counts by identifying connected components.

Methods	Training	Pascal-VOC		OmniCount-191	
		mRMSE	mRMSE-nz	mRMSE	mRMSE-nz
ILC [7]	✓	<u>0.29</u>	<u>1.14</u>	<u>4.56</u>	<u>9.39</u>
CEOES [3]	✓	0.42	1.65	-	-
Grounding-DINO [28]	✗	0.0066	0.05	1.29	3.27
CLIPSeg [31]	✗	0.0091	0.08	1.54	4.28
TFOC [42]	✗	0.0084	0.03	0.95	2.89
OmniCount	✗	0.0023	0.009	0.70	2.00

Table 1: Results in multi-label object counting setting using text prompts only. Best results in **bold** and underlined for the best scores for learning-based methods. OmniCount shows better performance even against training-based counterparts.

Results: In our comparative analysis, presented in Tab. 1, we benchmark our model against existing methods using the PASCAL VOC and OmniCount-191 datasets. The results demonstrate our approach’s superior performance, significantly eclipsing all baseline models. Notably, our training-free model outstrips all training-based baselines, highlighting the advantage of incorporating geometric insights into object counting. Such training-dependent models often suffer from limitations tied to their training datasets, affecting their adaptability in real-world scenarios. Our strategy effectively mitigates common obstacles like occlusions, which traditional detection and segmentation methods struggle with. Furthermore, our model’s ability to accurately count multiple object categories in a single forward pass distinguishes it from single-category models, which require a single pass for each category. This makes our model much more efficient (see Fig. 9) than all existing training-free counting models. It is also interesting to note that the SAM-based counting model outperforms the spectral-clustering-based counting model CLIPSeg baseline and bounding box-based counting baseline Grounding-DINO, re-verifying the effectiveness of SAM as a desired counting model. In Fig. 7, we visualize the results of OmniCount on PASCAL VOC and our curated OmniCount-191 datasets, while Fig. 8 offers a visual comparison with TFOC on OmniCount-191. These qualitative results showcase our model’s ability to count objects of varying sizes, from large singular items like horses and trains to medium-sized objects (*e.g.* boar, baskets etc.) and small, non-atomic entities like green peas and berries, highlighting OmniCount’s robustness and superior performance.

In Tab. 2, we report the performance of our model against TFOC [42] using both box and point prompts. This evaluation bypasses our reference point

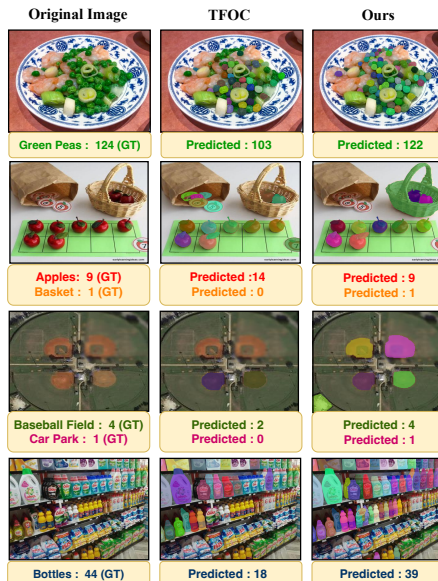


Fig. 8: Comparison of OmniCount against TFOC [42] on the OmniCount-191 dataset.

selection module, leveraging the ground truth bounding box and point annotations from the datasets as prompts for SAM. As shown in the table, our model too outperforms the baseline under this setting. Remarkably, the performance disparity between text-prompt and box-point-prompt settings for OmniCount is minimal, underscoring the robustness of our reference point selection strategy.

Prompt	Methods	Pascal-VOC		OmniCount-191	
		mRMSE	mRMSE-nz	mRMSE	mRMSE-nz
Box	TFOC	0.0067	0.018	0.91	2.78
	OmniCount	0.00185	0.00790	0.814	2.24
Point	TFOC	0.0072	0.025	0.917	2.85
	OmniCount	0.00190	0.00821	0.83	2.29

Table 2: Performance of various approaches in multi-label object counting setting using box and point prompts. The best results are in **bold**. OmniCount demonstrates better performance even against training-based benchmarks.

Models	Training Prompt		FSC-147				CARPK			
			MAE	RMSE	NAE	SRE	MAE	RMSE	NAE	SRE
CFOCNet+ [51]	✓	box	22.10	112.71	-	-	-	-	-	-
GMN [30]	✓	box	26.52	124.57	-	-7.48	9.90	-	-	-
BMNet+ [39]	✓	box	<u>14.62</u>	91.83	<u>0.25</u>	<u>2.74</u>	<u>5.76</u>	<u>7.83</u>	-	-
Vanilla SAM [18]	✗	N.A.	42.48	137.50	1.14	8.13	16.97	20.57	0.70	5.30
TFOC [42]	✗	box	19.95	132.16	0.29	3.80	10.97	14.24	0.48	3.70
OmniCount	✗	box	18.63	112.98	0.14	2.99	9.92	12.15	0.23	2.11
TFOC [42]	✗	point	20.10	132.83	0.30	3.87	11.01	14.34	0.51	3.89
OmniCount	✗	point	19.24	115.27	0.25	3.21	10.66	13.15	0.31	2.45
ZSOC [45]	✓	text	22.09	115.17	0.34	3.74	-	-	-	-
TFOC [42]	✗	text	24.79	137.15	0.37	4.52	-	-	-	-
OmniCount	✗	text	21.46	133.28	0.32	0.39	-	-	-	-

Table 3: Performance of OmniCount against competitors using text, point, and box prompts. The **bold** denotes the best among training-free methods, while the underlined font is the best among learning-based methods.

5.2 Single-label counting

Competitors: We report the performance of training-based methods like CFOCNet+ [51], GMN [30], BMNet [39], ZSOC [45] as well as training-free approaches like TFOC [42]. We have also adopted a SAM-based baseline for a fair comparison, reporting Vanilla SAM [18] counting results by processing entire images with a uniform point layout.

Results: We rigorously compare our model’s performance in a single-label context utilizing text, box, and point prompts, as detailed in Tab. 3. Similar to multi-label counting, OmniCount consistently outperforms the majority of training-based models, and all training-free models across all the text/box/point prompts modalities across four key metrics demonstrate its robustness and efficiency in object counting tasks. This also illustrates that merely using SAM as a counting model is inferior, even in single-class counting, highlighting the importance of semantic and geometric priors. More results and insights on other OmniCount-191 tasks, such as VQA, have been provided in the supplementary.

5.3 Further analysis

Counting efficiency: In assessing the scalability and efficiency of the existing training-free model TFOC and our OmniCount, we analyze their parameter counts and computational complexity. As shown in Fig. 9, TFOC’s parameters and GFLOPS increase exponentially with more object categories, while OmniCount shows linear growth as we only have class-specific SAM [18] component, which grows linearly w.r.t classes whilst other components remaining constant, signifying superior scalability and efficiency in diverse object scenarios.

Impact of depth refinement: OmniCount enhances SAM’s counting accuracy by incorporating two types of priors, namely semantic prior (SP) and geometric prior (GP). The findings from our experiment with the OmniCount-191 dataset are detailed in Tab. 4. Clearly, OmniCount w/o Geometric prior has 0.42/0.14% more error in m-RMSE/m-RMSE-nz metrics, indicating that SAM over-segments without structural information of occluded objects, which leads to over-counting.

Importance of reference points:

In Tab. 4, we assess the impact of the reference point selection algorithm on object counting using text as an exemplar within the OmniCount-191 dataset. We compare our OmniCount against a uniform point baseline from Vanilla SAM and OmniCount without Gaussian refinement. Results indicate that omitting Gaussian refinement increases m-RMSE/m-RMSE-nz error rates by 0.44/0.14%, suggesting quantization errors from upsampling F_P hamper SAM’s counting precision. Moreover, SAM’s default “everything mode” using uniform point selection increases over-counting, as shown by a 0.65/0.45% rise in error rates.

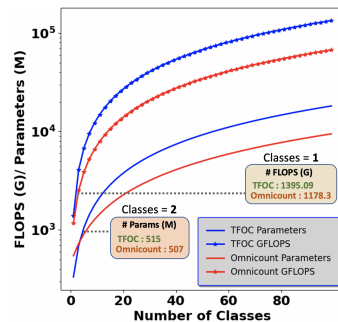


Fig. 9: Scalability versus efficiency plots of TFOC and OmniCount.

SP	GP	GR	RP	m-RMSE	m-RMSE-nz
✓	✗	✗	✗	3.21	4.95
✓	✗	✓	✓	0.74	1.82
✓	✓	✗	✗	0.97	2.13
✓	✓	✗	✓	0.53	1.99
✓	✓	✓	✓	0.32	1.68

Table 4: Ablation of different components on OmniCount-191 dataset. SP: Semantic Prior, GP: Geometric Prior, GR: Gaussian Refinement, RP: Reference Point

6 Conclusion

We introduced OmniCount, a novel open-vocabulary, multi-label counting model capable of processing multiple categories in a single pass, integrating semantic and geometric insights without requiring training. Surpassing traditional, category-specific models limited by dataset constraints, OmniCount utilizes pre-trained foundation models for semantic segmentation and depth estimation to address occlusions and achieve precise object segmentation and counting. To fill the void of a dedicated multi-label counting dataset, we developed OmniCount-191, featuring 30,230 images across 191 categories. OmniCount’s efficacy, tested

against existing benchmarks and our OmniCount-191 in various settings, showcases its superior performance, efficiency, and scalability, emphasizing its readiness for real-world applications and transforming multi-label counting into a feasible, practical tool.

References

1. Brown, T., Mann, B., Ryder, N., Subbiah, M., Kaplan, J.D., Dhariwal, P., et al.: Language models are few-shot learners. *NeurIPS* (2020) [3](#)
2. Bui, K.H.N., Yi, H., Cho, J.: A Vehicle Counts by Class Framework using Distinguished Regions Tracking at Multiple Intersections. In: *CVPRW* (2020) [1](#), [3](#)
3. Chattopadhyay, P., Vedantam, R., Selvaraju, R.R., Batra, D., Parikh, D.: Counting Everyday Objects in Everyday Scenes. In: *CVPR* (2017) [1](#), [3](#), [10](#), [11](#), [12](#)
4. Cheng, Z.Q., Dai, Q., Li, H., Song, J., Wu, X., Hauptmann, A.G.: Rethinking spatial invariance of convolutional networks for object counting. In: *CVPR* (2022) [3](#)
5. Cheng, Z.Q., Li, J.X., Dai, Q., Wu, X., Hauptmann, A.G.: Learning spatial awareness to improve crowd counting. In: *ICCV* (2019) [3](#)
6. Cheng, Z.Q., Li, J.X., Dai, Q., Wu, X., He, J.Y., Hauptmann, A.: Improving the learning of multi-column convolutional neural network for crowd counting. In: *ACM MM* (2019) [3](#)
7. Cholakkal, H., Sun, G., Khan, F.S., Shao, L.: Object counting and instance segmentation with image-level supervision. In: *CVPR* (2019) [1](#), [3](#), [10](#), [12](#)
8. Cholakkal, H., Sun, G., Khan, S., Khan, F.S., Shao, L., Gool, L.V.: Towards Partial Supervision for Generic Object Counting in Natural Scenes. *IEEE TPAMI* (2022) [1](#), [3](#), [10](#), [11](#)
9. Everingham, M., Gool, L.V., Williams, C.K.I., Winn, J., Zisserman, A.: The PASCAL Visual Object Classes (VOC) Challenge. *IJCV* (2009) [2](#), [11](#)
10. Gupta, S.K., Zhang, M., Wu, C.C., Wolfe, J., Kreiman, G.: Visual search asymmetry: Deep nets and humans share similar inherent biases. In: *NeurIPS* (2021) [3](#)
11. Han, T., Bai, L., Liu, L., Wanli, O.: STEERER: Resolving Scale Variations for Counting and Localization via Selective Inheritance Learning. In: *ICCV* (2023) [1](#), [3](#)
12. Hsieh, M.R., Lin, Y.L., Hsu, W.H.: Drone-based object counting by spatially regularized regional proposal network. In: *ICCV* (2017) [10](#)
13. Huang, Z.K., Chen, W.T., Chiang, Y.C., Kuo, S.Y., Yang, M.H.: Counting Crowds in Bad Weather. In: *ICCV* (2023) [1](#), [3](#)
14. Ji, G.P., Fan, D.P., Xu, P., Cheng, M.M., Zhou, B., Van Gool, L.: Sam struggles in concealed scenes – empirical study on “segment anything”. *SCIS* (2023) [4](#)
15. Jiang, R., Liu, L., Chen, C.: Clip-count: Towards text-guided zero-shot object counting. In: *ACM MM* (2023) [1](#)
16. Ke, B., Obukhov, A., Huang, S., Metzger, N., Daudt, R.C., Schindler, K.: Marigold: Repurposing diffusion-based image generators for monocular depth estimation. In: *CVPR* (2024) [4](#), [6](#)
17. Khan, A., Gould, S., Salzmann, M.: Deep Convolutional Neural Networks for Human Embryonic Cell Counting. In: *ECCV* (2016) [1](#), [3](#)
18. Kirillov, A., Mintun, E., Ravi, N., Mao, H., Rolland, C., Gustafson, L., Xiao, T., Whitehead, S., Berg, A.C., Lo, W.Y., et al.: Segment anything. In: *ICCV* (2023) [2](#), [3](#), [4](#), [5](#), [6](#), [7](#), [10](#), [13](#), [14](#)
19. Lempitsky, V., Zisserman, A.: Learning to count objects in images. In: *NeurIPS* (2010) [3](#)
20. Li, C., Hu, X., Abousamra, S., Chen, C.: Calibrating Uncertainty for Semi-Supervised Crowd Counting. In: *ICCV* (2023) [1](#), [3](#)

21. Li, Y., Zhang, X., Chen, D.: CSRNet: Dilated convolutional neural networks for understanding the highly congested scenes. In: CVPR (2018) [1](#), [3](#)
22. Lian, D., Chen, X., Li, J., Luo, W., Gao, S.: Locating and counting heads in crowds with a depth prior. IEEE TPAMI (2021) [3](#)
23. Lian, D., Li, J., Zheng, J., Luo, W., Gao, S.: Density map regression guided detection network for rgb-d crowd counting and localization. In: CVPR (2019) [3](#)
24. Liang, D., Xie, J., Zou, Z., Ye, X., Xu, W., Bai, X.: Crowdclip: Unsupervised crowd counting via vision-language model. In: CVPR (2023) [1](#), [3](#)
25. Liang, F., Wu, B., Dai, X., Li, K., Zhao, Y., Zhang, H., Zhang, P., Vajda, P., Marculescu, D.: Open-vocabulary semantic segmentation with mask-adapted clip. In: CVPR (2023) [5](#)
26. Lin, T.Y., Maire, M., Belongie, S., Hays, J., Perona, P., Ramanan, D., Dollár, P., Zitnick, C.L.: Microsoft coco: Common objects in context. In: ECCV (2014) [2](#), [8](#)
27. Liu, C., Lu, H., Cao, Z., Liu, T.: Point-query quadtree for crowd counting, localization, and more. In: ICCV (2023) [1](#), [3](#)
28. Liu, S., Zeng, Z., Ren, T., Li, F., Zhang, H., Yang, J., Li, C., Yang, J., Su, H., Zhu, J., et al.: Grounding DINO: Marrying DINO with Grounded Pre-Training for Open-Set Object Detection. arXiv preprint arXiv:2303.05499 (2023) [11](#), [12](#)
29. Long, J., Shelhamer, E., Darrell, T.: Fully convolutional networks for semantic segmentation. In: CVPR (2015) [6](#)
30. Lu, E., Xie, W., Zisserman, A.: Class-agnostic counting. In: ACCV (2019) [3](#), [13](#)
31. Lüddecke, T., Ecker, A.: Image segmentation using text and image prompts. In: CVPR (2022) [11](#), [12](#)
32. Luo, H., Bao, J., Wu, Y., He, X., Li, T.: Segclip: Patch aggregation with learnable centers for open-vocabulary semantic segmentation. In: ICML (2023) [5](#)
33. Radford, A., Kim, J.W., Hallacy, C., Ramesh, A., Goh, G., Agarwal, S., Sastry, G., Askell, A., Mishkin, P., Clark, J., et al.: Learning transferable visual models from natural language supervision. In: ICML (2021) [3](#)
34. Rahnmounfar, M., Sheppard, C.: Deep Count: Fruit Counting Based on Deep Simulated Learning. Sensors (2017) [1](#), [3](#)
35. Ranjan, V., Nguyen, M.H.: Exemplar Free Class Agnostic Counting. In: ACCV (2022) [1](#)
36. Ranjan, V., Nguyen, M.H.: Exemplar free class agnostic counting. In: ACCV (2022) [3](#), [5](#), [10](#)
37. Ranjan, V., Sharma, U., Nguyen, T., Hoai, M.: Learning to count everything. In: CVPR (2021) [1](#), [3](#), [8](#), [10](#)
38. Ranjan, V., Sharma, U., Nguyen, T., Hoai, M.: Learning to count everything. In: CVPR (2021) [3](#)
39. Shi, M., Lu, H., Feng, C., Liu, C., Cao, Z.: Represent, compare, and learn: A similarity-aware framework for class-agnostic counting. In: CVPR (2022) [3](#), [13](#)
40. Shi, Z., Mettes, P., Snoek, C.G.M.: Counting with focus for free. In: ICCV (2019) [3](#)
41. Shi, Z., Mettes, P., Snoek, C.G.: Focus for free in density-based counting. IJCV (2024) [3](#)
42. Shi, Z., Sun, Y., Zhang, M.: Training-free object counting with prompts. In: WACV (2024) [4](#), [5](#), [10](#), [11](#), [12](#), [13](#)
43. Shi, Z., Zhang, L., Liu, Y., Cao, X., Ye, Y., Cheng, M.M., Zheng, G.: Crowd counting with deep negative correlation learning. In: CVPR (2018) [3](#)
44. Song, Q., Wang, C., Jiang, Z., Wang, Y., Tai, Y., Wang, C., Li, J., Huang, F., Wu, Y.: Rethinking counting and localization in crowds: A purely point-based framework. In: ICCV (2021) [1](#), [3](#)

45. Xu, J., Le, H., Nguyen, V., Ranjan, V., Samaras, D.: Zero-shot object counting. In: CVPR (2023) [3](#), [5](#), [13](#)
46. Xu, J., Le, H., Samaras, D.: Zero-shot object counting with language-vision models. arXiv preprint arXiv:2309.13097 (2023) [5](#)
47. Xu, M., Zhang, Z., Wei, F., Hu, H., Bai, X.: Side adapter network for open-vocabulary semantic segmentation. In: CVPR (2023) [4](#), [5](#), [10](#), [11](#)
48. Xu, M., Zhang, Z., Wei, F., Lin, Y., Cao, Y., Hu, H., Bai, X.: A simple baseline for open-vocabulary semantic segmentation with pre-trained vision-language model. In: ECCV (2022) [5](#)
49. Xu, Y., Zhong, Z., Lian, D., Li, J., Li, Z., Xu, X., Gao, S.: Crowd counting with partial annotations in an image. In: ICCV (2021) [3](#)
50. Yang, S., Guo, W., Ren, Y.: Crowdfomer: An overlap patching vision transformer for top-down crowd counting. In: IJCAI (2022) [3](#)
51. Yang, S.D., Su, H.T., Hsu, W.H., Chen, W.C.: Class-agnostic few-shot object counting. In: WACV (2021) [3](#), [13](#)
52. You, Z., Yang, K., Luo, W., Lu, X., Cui, L., Le, X.: Few-shot object counting with similarity-aware feature enhancement. In: WACV (2022) [1](#), [3](#)
53. You, Z., Yang, K., Luo, W., Lu, X., Cui, L., Le, X.: Few-shot object counting with similarity-aware feature enhancement. In: WACV (2023) [3](#)
54. Zhang, F., Zhu, X., Dai, H., Ye, M., Zhu, C.: Distribution-aware coordinate representation for human pose estimation. In: CVPR (2020) [8](#)
55. Zhang, L., Shi, Z., Cheng, M.M., Liu, Y., Bian, J.W., Zhou, J.T., Zheng, G., Zeng, Z.: Nonlinear regression via deep negative correlation learning. IEEE TPAMI (2019) [3](#)
56. Zhang, M., Armendariz, M., Xiao, W., Rose, O., Bendtz, K., Livingstone, M., Ponce, C., Kreiman, G.: Look twice: A generalist computational model predicts return fixations across tasks and species. PLOS Comp. Bio. (2021) [3](#)
57. Zhang, M., Feng, J., Ma, K.T., Lim, J.H., Zhao, Q., Kreiman, G.: Finding any waldo with zero-shot invariant and efficient visual search. Nature Comm. (2018) [3](#)
58. Zhang, Y., Zhou, D., Chen, S., Gao, S., Ma, Y.: Single-image crowd counting via multi-column convolutional neural network. In: CVPR (2016) [3](#)